Biochemistry and Biophysics Reports 17 (2019) 197–207

Contents lists available at ScienceDirect

Biochemistry and Biophysics Reports

journal homepage: www.elsevier.com/locate/bbrep

Mannose-decorated hybrid nanoparticles for enhanced macrophage targeting

Elham Hatami[a], Ying Mu[b], Deanna N. Shields[c], Subhash C. Chauhan[a], Santosh Kumar[a], Theodore J. Cory[b,*], Murali M. Yallapu[a,**]

[a] Department of Pharmaceutical Sciences, College of Pharmacy, University of Tennessee Health Science Center, Memphis, TN 38163, USA
[b] Department of Clinical Pharmacy and Translational Science, College of Pharmacy, University of Tennessee Health Science Center, Memphis, TN 38163, USA
[c] Department of Chemistry, University of Memphis, TN 38152, USA

ARTICLE INFO

Keywords:
Nanoparticles
Mannose
Macrophage
HIV
Cancer

ABSTRACT

Our goal was to design nanocarriers that specifically target and deliver therapeutics to polarized macrophages. Mannose receptors are highly overexpressed on polarized macrophages. In this study, we constructed Pluronic® -F127 polymer and tannic acid (TA) based nanoparticles (F127-TA core nanoparticles) with varying mannose densities. The particle size of the optimized mannose-decorated F127-TA hybrid nanoparticles (MDNPs) was found to be ~ 265 nm with a negative zeta potential of ~ − 4.5 mV. No significant changes in the size and zeta potentials of nanoparticles were observed, which demonstrated structural integrity and stability of the nanoformulation. Physicochemical characteristics of MDNPs were evaluated by FTIR and TGA and demonstrated the presence of mannose units on surface nanoparticles. A mannose-dependent cellular targeting and uptake of MDNPs was found in U937 macrophages. The uptake process was found to vary directly with time and volume of MDNPs nanoparticles. The uptake pattern is higher in M2 than M1. This behavior was also evident from the instantaneous and superior binding profile of M2 macrophage lysate protein with MDNPs over that of M1 macrophage lysate protein. These results demonstrated that an appropriate mannose ligand density was confirmed, suggesting efficient targeting of M2. Altogether, these data support that the MDNPs formulation could serve as a targeted therapeutic guide in the generation of nanomedicine to treat various conditions as an anti-inflammation therapy.

1. Introduction

Macrophages play an important role in a variety of disease states, including cancer, fibrotic lung disease, cardiac disease, and a variety of infectious diseases, including HIV-1 [1–5]. Of note, macrophages can be activated over a range of phenotypes. On one extreme, exposure to a pro-inflammatory Th1 response polarizes them to the classically activated M1 phenotype. M1 macrophages are largely involved in phagocytosis of invasive pathogens and other extracellular particles. They largely produce proinflammatory cytokines, as well as reactive oxygen and reactive nitrogen species [5–7]. Macrophages are polarized to the M2 phenotype by cytokines produced from a Th2 immune response, and are largely involved in wound healing, tissue repair, and fibrotic repair after an acute inflammatory response, also in the response to many parasites. Macrophage polarization exists within a spectrum, with M1 and M2 representing the two extremes of this spectrum. Since macrophage function is widely associated with the response to a number of disease states, developing an efficient delivery platform capable of targeting and modulating the function of polarized macrophages may be a promising therapeutic approach.

Self-assembled units decorated with mannosides produces multifunctional supramolecular nanoparticles with remarkably higher entry, minimal cytotoxicity, and almost negligible cytokine production in macrophages. Nanosystems based on gold, quantum dot, gelatin, poly (lysine), and poly(propylene imine) were proven to be promising platforms for targeting macrophages [8–16]. Similarly, polymer nanosystems found to be a unique nanoparticle formulation that can be applied for wide variety medical applications. In this aspect, we

* Correspondence to: Department of Clinical Pharmacy and Translational Science, University of Tennessee Health Science Center, Room 342, 881 Madison Avenue, Memphis, TN 38163, USA.
** Correspondence to: Department of Pharmaceutical Sciences, University of Tennessee Health Science Center, Room 447, 881 Madison Avenue, Memphis, TN 38163, USA.
E-mail addresses: tcory1@uthsc.edu (T.J. Cory), myallapu@uthsc.edu (M.M. Yallapu).

https://doi.org/10.1016/j.bbrep.2019.01.007
Received 21 December 2018; Received in revised form 11 January 2019; Accepted 16 January 2019
Available online 25 January 2019

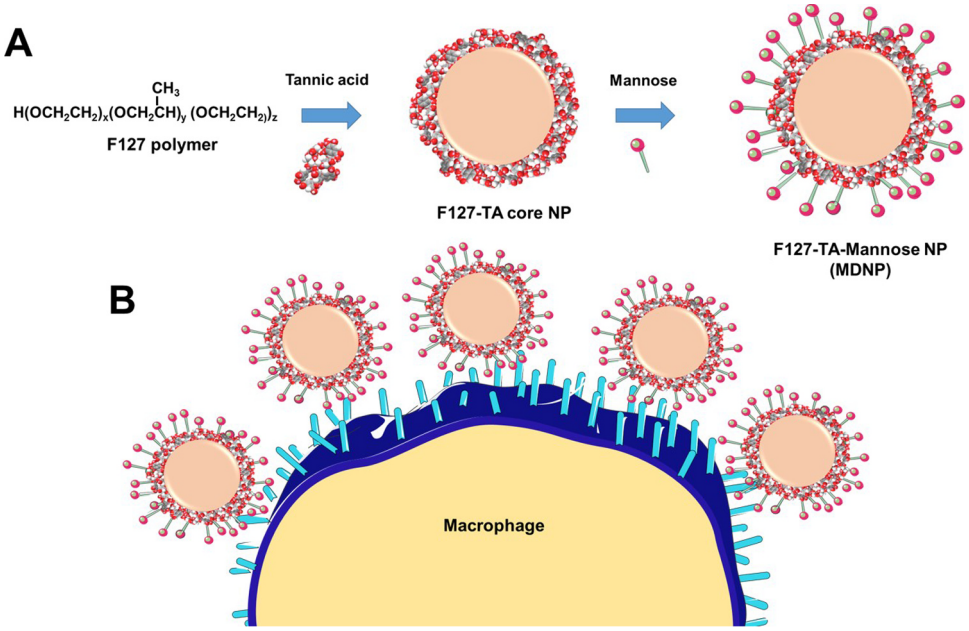

Scheme 1. Schematic representation of (A) generation of mannose-decorated nanoparticles (MDNPs) and (B) possible receptor mediated binding of MDNPs with macrophages.

envision that a unique and simple mannose-decorated nanoparticle system which does not use an excessive amount of organic solvents and extensive synthetic chemistry for production would be highly attractive.

In this study, we report a mannose-decorated hybrid nanoparticle system with appropriate density for superior targeting of M2 over M1. Mannose decoration was achieved via a simple self-assembly process, in which F127-polymer (F127, a PEG-PPO-PEG co-polymer) and tannic acid (TA) layers are physically crosslinked with the hydroxyl groups of mannose. We choose F127 as a polymer as one of nanoparticle core generation material because it is 1) a nonionic surfactant molecule (no systemic toxicity), 2) superior miscibility/compatibility with number of substances (therapeutic molecules), and 3) solubility enhancer for number of drug molecules, which offers excellent delivery carrier, and 4) delivery platform for a number of routes of administration [17–21]. Tannic acid was proposed as other core forming material due to 1) it is a safe plant extracted polyphenolic compounds which is widely used as an alternative surface modifier, 2) it interacts with a number of oligomers and polymers (including F127 polymer) via covalent and non-covalent interactions, 3) it binds to molecules/cells by interacting with hydroxyl-, carboxyl-, amine- or thiol groups, and 4) offers layer-by-layer self-assembly generating platforms for drug delivery application [22–25]. Another important reason to use this combination is because F127 and TA are “generally recognized as safe (GRAS)” molecules by US Food and Drug Administration. The other reason to use F127 (PEG-PPO-PEG co-polymer) is that TA has higher binding efficiency over other polymers such as poly(vinyl alcohol) or poly(vinyl pyrrolidone) [26]. To study specific targeting of MDNPs on MR of macrophages, we choose the U937 cells as a model cell line which is commonly used in biomedical research, including pharmacology studies [27,28]. We have also extensively used this cell line, and shown that they are phenotypically similar to activated M1 and M2 monocyte derived macrophages [29,30].

We confirmed that the MDNPs are successfully localized on the surface of M2 and internalized in a dose- and time-dependent manner. These nanoparticles exhibited an accelerated interaction and distribution within the cytoplasmic compartment of macrophages, which can then deliver therapeutics in an efficacious fashion. Overall, these results prompted us to apply MDNPs to targeted delivery to M2, which could play a role in the treatment of a number of disease states.

2. Materials and methods

2.1. Methods

U937 cells were utilized for all cell culture experiments. RPMI 1640 supplemented with 10% FBS was used for U937 cell culture. U937 cells were purchased from American Type Culture Collection (ATCC Manassas, VA). Cells were polarized to the M1 or the M2 phenotype using protocols we have previously developed [29,30]. Cells were polarized to the M1 phenotype with 48 h of treatment of LPS (100 ng/mL, E. Coli origin, Sigma-Aldrich, St. Louis, Mo, USA) combined with INF-γ (20 ng/mL, Life Technologies, Carlsbad, CA, USA). Forty-eight hours of LPS (100 ng/mL) with IL-4 (10 ng/mL, CST, Danvers, MA, USA) and IL-13 (10 ng/mL, CST, Danvers, MA, USA) treatments were used for M2 polarization.

2.2. Generation of MDNPs

F127-polymer and tannic acid (F127-TA) nanoparticles decorated with different mannose densities were prepared by a self-assembly process. This was achieved in a two-step process. The first step involved simultaneous mixing of 100 μg F127 (100 μL of 1 mg/mL F127 solution) and 100 μg TA (100 μL of 1 mg/mL TA solution) dissolved in 1 mL of water with 400 rpm stirring in a 10 mL glass vial (#FS60910A-2, Fisher Scientific, Grand Island, NY) to construct the F127-TA cores of the nanoparticles in aqueous suspension. This core nanoparticle suspension was subjected to probe sonication (200 W, VirSonic Ultrasonic Cell Disrupter 100, The VirTis Company, Woburn, MA) for 2 min in order to achieve a uniform sized core nanoparticle solution. In the second step, mannose (5 mg/mL) was added into the F127-TA core nanoparticle solution at a predetermined feed with various mass ratios (0.25:1, 0.5:1, 0.75:1, 1:1, 2.5:1, mannose: core nanoparticles) for 24 h at room temperature under magnetic stirring (400 rpm) (MS-H-S10, Scilogex, Rocky Hill, CT). Unbound mannose on nanoparticles were removed in supernatant by centrifugation process (5000 rpm in Sorvall ST 8 Centrifuge, Thermo Fisher Scientific, Suzhou, China). Mannose decoration on F127-TA nanoparticles and its feasible macrophage targeting was represented

Table 1
Composition and physical parameters of MDNPs.

MDNPs code	Mean particle size (nm)	Zeta potential (mV)	Mannose density (μg) in MDNPs along with respect to 200 μg of F127-TA core
MDNPs 0	131.9	−9.09	0
MDNPS 50 (0.25:1)	206.7	−11.1	48.2
MDNPS 100 (0.5:1)	207.9	−4.6	96.5
MDNPS 150 (0.75:1)	281.0	−3.4	146.8
MDNPS 200 (1:1)	265.9	−4.5	195.4
MDNPs 500 (2.5:1)	325.1	−4.11	280.6

MDNPs (number) suffix indicates amount of mannose used in generation of MDNPs along with 200 μg of F127-TA core NPs.
Note: For convenience MDNPs 200 formulation represented as MDNPs with 200 mannose density for convenience and all physicochemical characterization were presented for this formulation.

schematically in Scheme 1.

2.3. Physicochemical characterization

The hydrodynamic particle size, particle size distribution, and zeta potential of hydrated nanoparticles in aqueous solution were monitored by dynamic light scattering (DLS) using Zetasizer (Nano ZS, Malvern Instruments, Malvern, UK). All particle size and zeta potential measurements of nanoparticles were acquired following our established protocol [31,32]. In brief, first freshly generated F127-TA core or MDNPs suspensions (50 μL) were diluted to 1 mg/mL with milli-Q water (~ 154 mM and pH ~ 7.4). A short span (30 s) of tip sonication (VirSonic Ultrasonic Cell Disrupter 100, VirTis, Woburn, MA, USA) was applied to ensure to achieve a homogeneous particle suspension just before measurements. Particle size measurements were performed in water for 3 min at 25 °C. A cumulative and average diameter and distribution of particle size was reported in Table 1 from triplicated runs. In addition, stability of formulations was determined by Zeta potential measurements. Zeta potential (ζ, mV) measurements were performed using laser Doppler velocimetry method. Acquisitions were done for three measurements of 20 runs with a gap of 120 s equilibrium time and data was presented as an average of triplicate measurements. All of the measurements were performed in triplicate.

The dry state size and morphology of F127-TA core nanoparticles and MDNPs were characterized by transmission electron microscopy (JEOL 200EX TEM, JEOL Ltd, Tokyo, Japan) operating at 80 kV. For preparation of nanoparticles on grids for TEM imaging, 100 μL of sample was dispersed in milli-Q water in 1:10 ratio, sonicated for 30 s, and then a 20 μL aliquot of the resulting imaging sample was carefully placed on the shiny side of the 200-mesh standard TEM grid (Electron Microscopy Science). A uranyl acetate solution (#22400, Electron Microscopy Sciences, Hatfield, PA) followed by 2X washing was used to enhance the contrast property of the nanoparticles. Imaging of dried nanoparticles on the grid was acquired following our published procedure [32]. FT-IR spectral data of nanoparticles were acquired using PerkinElmer Spectrum 100 FTIR spectrometer (Waltham, MA, US) equipped a diamond Attenuated Total Reflection crystal plate [23]. Approximately 2 mg of lyophilized samples were directly placed on the sample holder and the spectral information was recorded from 4000 cm^{-1} and 650 cm^{-1} with a resolution of 4 cm^{-1}. Spectral data was presented as an average of 32 scans. Further, the phenol-sulfuric acid assay was employed to assess the amount of mannose crosslinked on to nanoparticles [33]. F127-TA core nanoparticles was employed as control in this assay. Mannose standards were made within limitations. The color development in the phenol-sulfuric acid assay was recording on a plate reader at wavelength of 490 nm. The content of mannose on nanoparticles (μg/μg) was calculated by normalization with the nanoparticle mass. The thermal history of nanoparticles was examined using a Perkin Elmer Simultaneous Thermal Analyzer STA6000 [34].

2.4. Macrophage affinity of MDNPs

A fluorescence quenching assay was utilized to study the affinity of F127-TA core nanoparticles, mannose alone, and MDNPs with macrophages. The extent of affinity can be determined by the ability of MDNPs to reduce protein tryptophan residues [34]. For this study, 100 μg protein lysate of M1 or M2 phenotype dispersed in 1 mL 1X PBS were used to interact with 50 μg of mannose or nanoparticle solution in a 10 mm path length quartz cuvette (1.5 mL). The fluorescence measurements were carried out using a SpectraMax Plus plate reader (Molecular Devices, Sunnyvale, CA, USA) in the wavelength range of 250–450 nm at an excitation wavelength of 280 nm.

2.5. Macrophage targeting efficiency of MDNPs

In order to evaluate the macrophage targeting efficiency of nanoparticles, we labeled F127-TA core nanoparticles and MDNPs with coumarin 6 (C6), following our established method [32]. In detail, C6 in acetone (stock concentration, 1 mg/mL) was slowly added to 100 μg F127 (100 μL of 1 mg/mL F127 solution) and 100 μg TA (100 μL of 1 mg/mL TA solution), followed by sonication, various feed ratios of mannose were introduced into the formulation mixture as detailed in Section 2.2. The formulation was stirred for 24 h at room temperature using a magnetic stirrer to achieve C6-labeled-MDNPs. At the end, unbound mannose/dye in nanoparticles were removed in supernatant by centrifugation. Note: Since, C6 is a fluorescent dye, and can be leached out from F127-TA core. To minimize the leaching factors in this study, we performed uptake studies the early time points of 1, 3, and 6 h. In addition, if the dye is leached out from nanoparticles, it can be clearly seen as crystals due to precipitation in the aqueous cell culture medium. Note: We scaled up the MDNPs 200 formulation up to 2 g batches with reproducibility of 5–10% variation in particle size.

Coumarin 6 labeling enables rapid visualization and detection of nanoparticles in cells. The targeting efficacy experiment was performed in two distinct in vitro cellular binding methods (microscope visualization and flow cytometry). For these tests, U937 cell line-differentiated M1 and M2 macrophages were seeded in 6-well plates (5×10^5 cells/well) 24 h before experiments. Cells were co-incubated with 50 μL of C6-labeled-F127-TA core nanoparticles or C6-labeled-MDNPs for 3 h. This study first optimized for the superior uptake or binding of MDNPs compared to F127-TA core nanoparticles by employing different mannose-decorated nanoparticles (MDNPs) (mannose density was 0, 50, 100, 150, 200 μg containing MDNPs) while maintaining the same amount of C6, incubation time was 3 h). The study was then extended for time-dependent (1, 3, and 6 h for a mannose density (200 μg) in MDNPs 5 μg of C6). After treatments, cells were subjected to 2X PBS wash, then fresh RPMI phenol red-free medium was added to the cells, and the uptake results of the C6-labeled nanoparticles in cells were imaged using EVOS® FL Imaging System (AMF4300, Life Technologies, Carlsbad, CA, USA). Under the same conditions and treatment groups, cells were collected for flow cytometry in RPMI phenol red-free medium and nanoparticle binding/internalization in cells were

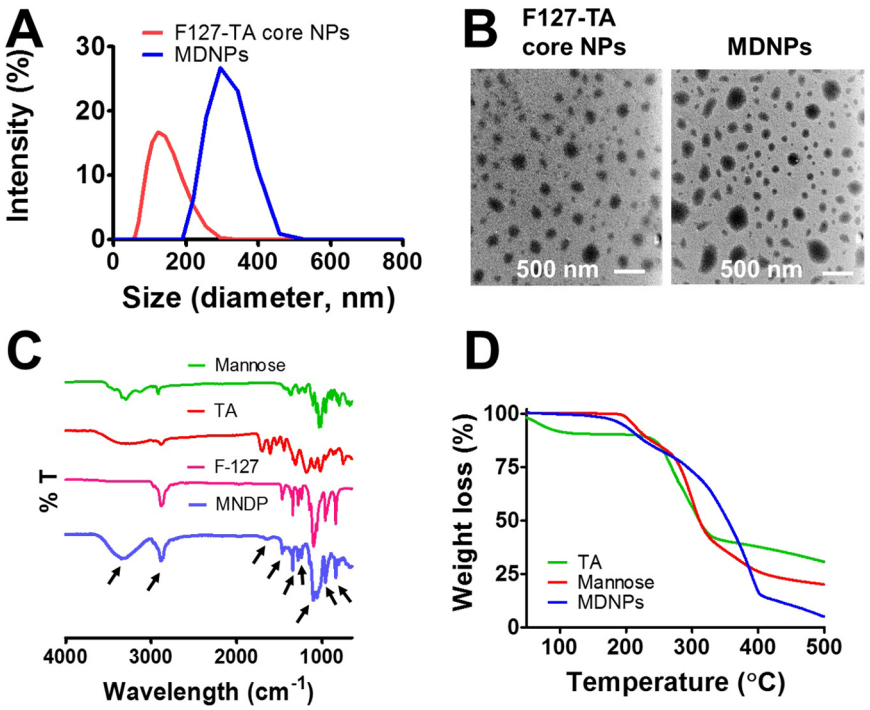

Fig. 1. Physicochemical characterization of MDNPs. **(A)** Hydrodynamic particle size distribution and zeta potentials of MDNPs measured by DLS. Data is representative of three independent measurements. **(B)** Morphology of bare F127-TA core nanoparticles and MDNPs. Scale bar was 500 nm. TEM image is representation from 10 different fields for each sample. **(C)** FT-IR spectra of MDNPs exhibiting functional group peaks relevant to F127 polymer, tannic acid and mannose. **(D)** Thermogravimetric profile of MDNPs indicating distinct from parent tannic acid and mannose.

quantified using the NovoCyte Flow Cytometer (ACEA NovoCyte® 1000, ACEA Biosciences, Inc. San Diego, Ca, USA) in FITC channel (fluorescence measurements at λ_{ex}: 485 nm and λ_{em}: 520 nm). 10,000 cells were subjected into flow cytometer to measure mean intensity fluorescence of dye contained MDNPs in each cell. The mean fluorescence intensity and standard deviations were determined from triplicate measurements.

2.6. Cytocompatibility of MDNPs in U937 cells

To investigate cytocompatibility, a cell viability assay using an MTS assay (CellTiter 96® AQueous, Promega, Madison, WI) was performed. Polarized U937 cells (5×10^3 per well) were seeded in 96-well plates. After 24 h, cells were treated with 0–200 μg/mL of F127-TA core nanoparticles or MDNPs in medium for 24 h. Then, cells were incubated with 20 μL MTS reagent in each well and allowed to develop color for 2 h at 37 °C. The absorbance of developed color is proportional to cell growth, and this was measured at 490 nm in a microplate reader (BioTeK Cytation 3, Winooski, VT, USA). The effect of nanoparticles on the cell growth of U937 was measured as the percentage of cell viability, where control cells (no treatment group) was considered 100% viable.

2.7. Statistical analysis

The statistical software Graph Pad 5.03 version (GraphPad Software, Inc., La Jolla, CA, USA) was employed to calculate average and standard error of mean from at least three readings of data. All cellular binding and target experimental data were used to determine statistical significance among treatment groups or between M2 and M1 phenotype cells by two-tailed student test; a p-value less than 0.05 was considered to be significant.

3. Results

The objective of this study was to generate a facile nanoparticle formulation with a precise targeting motif in its architecture. Mannose is a simple sugar carbohydrate which has major roles in the chemistry and metabolism in mammalian cells and tissues [35]. This molecule primarily serves as the molecular recognition of mannose receptors on cells of the innate immune system, including macrophages [36–38]. Considering this fact, we generated mannose-decorated F127-TA hybrid nanoparticles, referred to as MDNPs, through a self-assembly process (Scheme 1).

Nanoparticles of varying mannose densities with a feed mass ratios (0.25:1, 0.5:1, 0.75:1, 1:1, 2.5:1, mannose: core nanoparticles, core nanoparticles remains constant amount i.e., 100 μg F127 + 100 μg TA) were prepared. In all formulations, physically/loosely bound mannose moieties on MDNPs were removed by centrifugation at 5000 rpm for 5 min. The mannose density on F127-TA core nanoparticles was determined by the phenol-sulfuric acid assay. The mannose content on MDNPs were found to be 48.2, 96.5, 146.8, 195.4, and 280.6 μg density when we employed mannose feed 50, 100, 150, 200, and 500 on F127-TA nanoparticle core (Table 1). In most of the MDNPs mannose is incorporated more than 90% of feed except MDNPs 500 formulation. The particle sizes, particle size distributions, and zeta potential of MDNPs were in the range of ~ 131–325 nm and −11.00 to −3.4 mV. Poor stability of a formulation can be determined as its zeta potential closer to zero. When the zeta potential is positive or negative those formulations achieve maximum stability. From our data, it is apparent that the low negative zeta potential certainly offer good stability to MDNPs over time.

3.1. Physicochemical characterization of MDNPs

F127-TA core nanoparticles possessed an average particle size of ~ 131 nm with a polydispersity index of 0.19 (Fig. 1A). When these core nanoparticles were decorated with varying mannose densities, they exhibited average particle size of ~ 206–379 (polydispersity index (PDI) < 0.2). An optimum mannose coating (200 μg) on F127-TA core nanoparticles showed average particle size of ~ 265 nm. This indicates that mannose molecules are tightly embedded onto the F127-TA core nanoparticles without changing their particle sizes. This can be observed visually in TEM images of F127-TA and MDNPs. The spherical shapes of nanoparticles of F127-TA core nanoparticles are slightly altered by deposition of mannose molecules without altering their particle sizes (Fig. 1B). Both types of nanoparticles revealed a well-dispersed and spheroidal structural morphology.

Measurements of zeta potential using DLS were employed to characterize the mannose decoration on nanoparticles. F127-TA core nanoparticles showed -9.097 ± 1.128 mV while various degrees of mannose functionalization on F127-TA core nanoparticles exhibited values in the range of -2.517 ± 0.564 to -11 ± 0.666 mV. The shift in charge on nanoparticles can be attributed to the deposition of mannose on the surface of nanoparticles. A similar charge variation was observed after functionalization with mannose on lipid and solid nanoparticles [39,40]. Negative zeta potentials can cause strong repellent forces among the particles to prevent agglomeration and less systemic toxicity. Overall these physicochemical characteristics are helpful for rendering MNDP more stable and biocompatible for further studies.

The successful incorporation of mannose molecules onto F127-TA core nanoparticles was confirmed through determination of their chemical composition by FTIR spectroscopy. Before, performing FTIR acquisitions, loosely bound mannose on MDNPs were removed by centrifugation at 5000 rpm for 5 min. The spectra of mannose, tannic acid and F127-TA and MDNPs were presented in Fig. 1C. The FTIR spectrum of the F127 showed a visible characteristic band at 1010 cm^{-1} assigned to the CH_2 rocking and C–O–C stretch vibrations of ethylene glycol/propylene glycol chains F127 polymer. FTIR spectrum of TA exhibited a characteristic bands at 1700 cm^{-1}, 1603 cm^{-1}, and 1198 cm^{-1} belong to C=O, aromatic C=C, and phenolic C=O stretching for tannic acid. Characteristic peak of mannose was noticed at 1059 cm^{-1}, 1070 cm^{-1}, 1090 cm^{-1} due to C-OH stretching. In the case of MDNPs spectrum, combination of these peaks were appeared (shown as small arrows in the graph). This is a direct evidence of incorporated mannose sugar units on the F127-TA core nanoparticles leading to MDNPs. In addition, TGA profiles of MDNPs shows distinct than TA and mannose alone. The degradation characteristics of TA shows even at 50 °C but afterwards follows similar as mannose. MDNPs shown higher degradation pattern after 225 °C due to the presence of F127 polymer.

3.2. MDNPs exhibited molecular affinity towards M2 phenotype macrophages

Nanoparticles composed of mannose units in their structure are widely employed in delivery of therapeutics and tissue engineering applications. The mannose receptor is an integral membrane protein which facilitates the uptake of various glycoproteins (L-fucose, D-mannose, or N-acetylglucosamine). Thus mannose can interact with MR containing cells. Such interaction often lead to the formation of a protein corona on MDNPs due to specific interactions [41,42]. To verify this phenomenon, we examined the molecular affinity of MDNPs against cell lysates of macrophages (Fig. 2). In this method, intrinsic fluorescence of proteins are compared with the change of environment around tryptophan (Trp) residues [23,32] by employing either core nanoparticles or MDNPs. The principle of this technique allows us to measure decay of Trp fluorescence intensity due to binding with mannose molecules or buried within mannose layers on MDNPs compared to unexposed Trps. A control protein lysate fluorescence spectra is presented in Fig. 2 as black color curves. The core F127-TA nanoparticles (no mannose) demonstrated a decrease in the fluorescence peak indicating some degree of interactive affinity against M1 and M2 macrophages, which may be due to tannic acid binding to a number of different proteins in macrophages. However, MDNPs significantly brings down further fluorescence spectral peak (Fig. 2B, red color) which is an indication for a greater interaction affinity against M2 compared to M1 (Fig. 2A, red line curves). Statistical analysis is further confirm this evidence (Fig. 2C). This indicates a greater and more spontaneous molecular recognition of mannose receptors via biological cross-linking of MDNPs with M2 than is observed with M1.

3.3. MDNPs targets M2 phenotype macrophages

Mannosylated compounds, macromolecules, and nanoparticles often undergo specific interaction with mannose receptors (CD206) on cells, which involves receptor-mediated endocytosis and internalization into cytoplasmic compartments. Such biological processes have been reported in the case of various nanoparticles targeted delivery to macrophages [8–16]. To confirm such specific interactions between MDNPs and U937 cells, we performed a series of uptake assays by varying mannose density on F127-TA nanoparticles and their time-dependent interaction with cells (Figs. 3 and 4).

In this study, M1- and M2-differentiated macrophages of U937 cells were used, and C6 dye in nanoparticles was used to track MDNPs in cells. There is a possibility that C6 (fluorescent dye) can be leached out from MDNPs over period of time. With our previous experience, it occurs heavily overnight or after 24 h of incubation in cell culture. Therefore, to minimize this aspect in our uptake studies, we performed experiments only up to 6 h. If any dye leach out MDNPs, it can be observed as a crystal since C6 precipitates in aqueous cell culture medium.

Visual evidence from fluorescence images of nanoparticles in cells revealed that F127-TA core nanoparticles exhibited a low amount of uptake of nanoparticles in both M1 and M2 (Fig. 3A). When these core nanoparticles were decorated with mannose at varying densities, a dose-dependent significant uptake was noticed both in M1 and M2 U937 macrophages (Fig. 3A). However, the uptake was significantly higher in M2 compared to M1 (Fig. 3A). The exact pattern of higher uptake in M2 compared to M1 was observed with MDNPs in flow cytometry analysis (Fig. 3B-C). Flow cytometry analysis is more accurate and uses a broader cumulative representation of 10,000 cells. Such higher molecular recognition suggests that the mannose units on F127-TA nanoparticles have aligned on surface of F127-TA core nanoparticles and but are not buried in the polymer layers of core nanoparticles that are favorable for recognizing mannose receptors on U937 cells. It should be noted that flow cytometry results measure mean fluorescence intensity (MFI) (fluorescence levels) in cells due to dye in MDNPs. MFI is proportional to the extent of binding affinity. More MFI value is an indicative of high affinity. This suggests that mannose conjugation on nanoparticles ultimately dictate the fate of targeting U937 cells. Additionally, higher amounts than 200 μg of mannose on nanoparticle did not yield superior uptake there 200 μg of mannose was fixed for our future uptake and biocompatibility studies. Additional experiments utilizing visual evidence (Fig. 4A) and flow cytometry data (Fig. 4B-C) of time-dependent uptake showed significantly higher uptake with MDNPs compared to F127-TA core nanoparticles (Fig. 4). This pattern was true in both M2 and M1 U937 cells. However, as was observed with the fluorescence experiments, there was significantly higher uptake of MDNPs in M2 U937 cells compared to M1 cells.

At all tested concentrations and time points, the internalization of MNDPs are significantly higher in M2 over M1 macrophages. Such spontaneously-formed nanoparticles are promising nanosystems to depot and deliver therapeutic agents in both local and systemic bacterial infections. Additionally, this is our first evidence that the MDNPs formulation can be implemented for future targeting of infection diseases.

3.4. MDNPs exhibit cytocompatibility

To examine cytocompatibility of F127-TA and MDNPs, we employed a U937 cell viability assay. Polarized U937 cells treated with various concentrations 0–200 μg of nanoparticles for 24 h showed similar cell growth as found in control cells (Fig. 5A). Additionally, no significant decrease in the proliferative activity of cells was observed even at the highest concentration employed. This behavior was confirmed in morphological examinations using microscopy. Microscopic images of cells before and after treatment showed no significant change (Fig. 5B). This indicates that both core and mannose-decorated nanoparticles are cytocompatible. Taken together, the data generated from this study supports the interpretation that MDNPs are cytocompatible and capable of targeting polarized macrophages (U937).

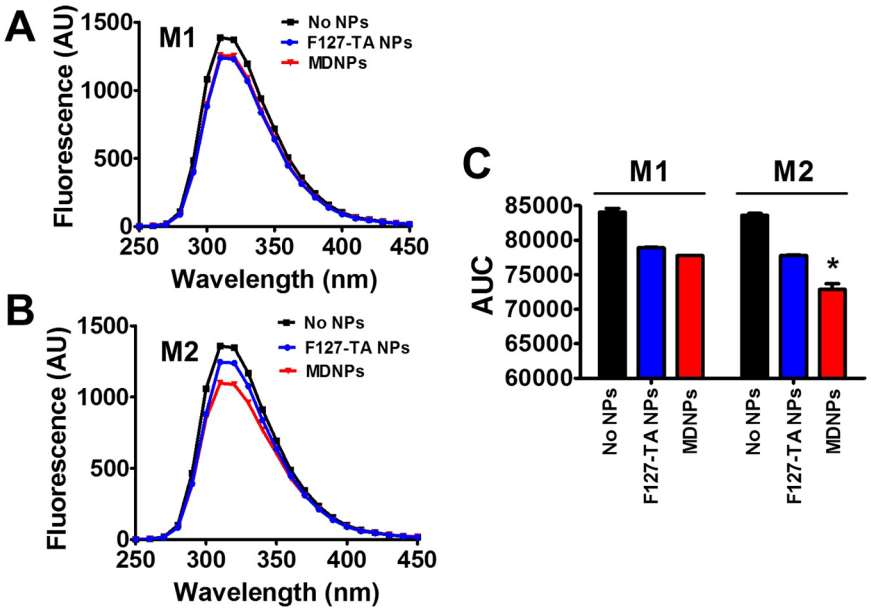

Fig. 2. MDNPs exhibits superior binding affinity to U937 cell line-differentiated M2 compared to M1 macrophage proteins. Fluorescence spectral data of **(A)** M1 macrophage proteins and **(B)** M2 macrophage proteins. Fluorescence intensity decrease is an indication for interaction between protein lysates and NPs. **(C)** Area under the curve of fluorescence data of A-B provides statistical significance with M2 macrophage protein quenching with MDNPs but not M1 macrophage protein lysate. Data represents mean ± SE (n = 3).

4. Discussion

Various infectious disease treatments have been significantly improved with awareness and earlier diagnosis. Scientific evidence has uncovered the important role of macrophages in various disease states [43–46]. Interestingly, polarized macrophages are believed to be involved in the initiation and progression of disease [45–48]. Macrophages are one of the potential targets for treatment and diagnosis of chronic infectious diseases [44–48]. Macrophages highly overexpress the mannose receptor CD206 on cell membranes [36–38]. One of the primary carbohydrate binding receptors, CD206 is an endocytic 175-kDa trans-membrane protein consisting of three extracellular regions (C-type lectin carbohydrate-recognition domains, NH_2-terminal cysteine-rich domain, and a fibronectin II domain). These domains can be recognized as having a higher affinity with mannose interaction/binding with sulfated carbohydrates or cysteine residues. Therefore, this study was directed toward developing a targeted mannose-decorated nanoformulation, which would present a key opportunity for the management of several inflammatory diseases.

Construction of nanoparticles with a suitable target motif offers a novel approach for a rational design for effective therapeutic delivery purposes. Such construction often requires harsh chemical/solvent use and multiple synthetic reactions, which tend to increase particle size and compromises stability. To overcome these issues, we followed a simple self-assembly process based on our previous successful drug nanoformulation (Scheme 1). The MDNP formulations achieved herein demonstrate a unique design of tannic acid-pluronic polymer core with mannose self-assembly fabrication that allows for the targeting of macrophages.

In this study, we examined the binding characteristics of mannose and mannose-decorated nanoparticles via internalization by polarized U937 cells at various mannose densities on nanoparticles, and in time-dependent manners using microscopic, flow cytometry, and spectrofluorometry methods (Figs. 2-4). In these analyses, mannose decorated NPs showed significantly higher binding with M2 phenotype macrophages compared to M1 phenotype macrophages. Moreover, this binding capacity was confirmed with an instantaneous protein and nanoparticle interaction using steady-state fluorescence measurements (Fig. 2). These data support the interpretation that our nanoparticles have specificity and interaction capacity with the cell surface of CD206 that present heavily with M2 phenotype macrophages.

Nanoparticles provide distinct advantages for therapeutic application over traditional delivery methods by improving the targeted efficacy, pharmacokinetics, and bioavailability of the drugs being delivered. Functionalization of an active targeting motif creates opportunity and allows superior targeting of monocytes and macrophages with a high specificity and affinity [8–16]. Major criteria for construction of such active targeted nanosystems are high ligand density and a favorable orientation for the ligand. Our study demonstrated that a 1:1 mannose: NPs ratio (200 μg manse density on nanoparticles) density on the constructed nanoparticles represented a minimal threshold for initiating the ligand-receptor-mediated interaction.

Infected macrophages often exhibit certain receptors which can be used for receptor-mediated targeted delivery applications. These receptors offer harboring of surface-modified nanocarriers for targeting macrophages that are necessary for the treatment of macrophage-associated diseases or vaccination purposes. Such targeting of nanocarriers in macrophages not only acts as a secondary depot of therapeutics, but also facilitates long-term localized delivery at the infection site. Our MDNPs-targeted delivery explores the concept that mannose receptors are superior for various drug delivery carriers due to the possibility of using simple self-assemblies of polymer nanoparticles and mannose. Additionally, U937 cells treated with the MDNPs developed for this study exhibited over 95% viability when treated at concentrations ranging from 0 to 200 μg/mL. The results suggest the adequate biocompatibility of MDNPs, which can be feasible for implementing in vivo testing in our future translational experiments. Although all MDNP formulations were produced at lower concentration batches (mg) but considering preparative process it is possible to scale up without using any sophisticated equipment up to 10–100 g scale. However, scale up process needs to verify for similar physico-chemical and targeting phenomenon aspects.

Polarized macrophages play an important role in a variety of disease states. A nanoformulated delivery system with the ability to target both classically and alternatively activated macrophages has the high potential for being beneficial in a variety of disease states. Of note, such delivery systems may have value for the treatment of obesity, cancer, inflammatory lung disease, and infectious diseases [49–52]. In addition to utility in infectious diseases including tuberculosis and *pseudomonas* pneumonia, there is evidence that targeting the macrophages may have utility in combating HIV.

In individuals infected with HIV-1, CD4 T-cells represent a reservoir for the retrovirus, and macrophages can also function as a cellular reservoir for HIV-1. Macrophages represent a long-lived sanctuary for HIV

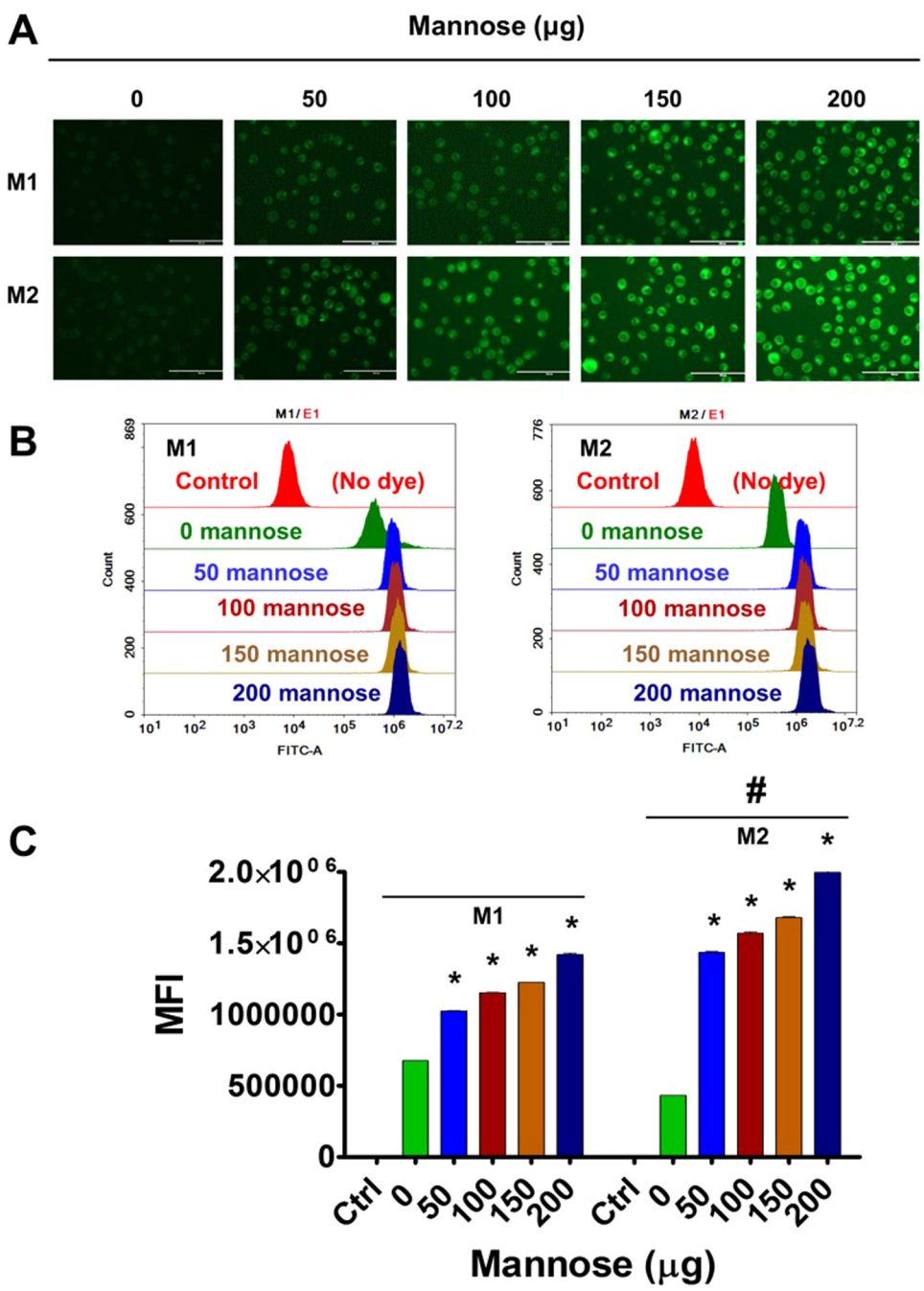

Fig. 3. MDNPs demonstrate specific binding to U937 cell line-differentiated M1 and M2 macrophages. 5×10^5 cells were treated with 0–200 μg/mL mannose density on MDNPs (but maintained C6 concentration as 5 μg/mL in every treatment) for 3 h. Then medium was replaced with fresh medium (no phenol red). **(A)** The uptake pattern of MDNPs in cells was imaged under EVOS® FL Imaging System (AMF4300, Life Technologies, Carlsbad, CA, USA) and **(B-C)** semi-quantitation of cellular binding of MDNPs was acquired by flow cytometer NovoCyte Flow Cytometer. The mean fluorescence intensity (MFI) values were presented as Data are mean ± SEM (n = 3). Significant p-values (< 0.05) are represented as "*" different mannose density treated cells compared to control cells. Significant p-value (< 0.05) is represented as "#" M2 cells compared to M1 at individual mannose density treatment.

infection in tissue sites including gut-associated lymphoid tissue and the brain [53,54] and are necessary sites for antiretroviral therapy (ART) [55–60]. Infected macrophages are believed to be cells in which an HIV infection is productive and less cytotoxic [4,61]. In HIV, the role of the two specific subsets of macrophage is complex. The cytokines produced by M1 macrophages drive increased viral replication and tissue damage, while the cytokines produced by M2 activation decrease viral replication [45,62]. The general inflammatory state induced by an active HIV infection may further drive unpolarized macrophages towards the M1 phenotype, allowing for increased viral infectivity and viral production [63]. There is thus considerable interest in developing nanoformulations which can target macrophages, either to directly combat viral replication in the macrophage reservoir, or as a mechanism to target other cellular reservoirs of HIV, and a variety of different strategies are in development [64,65].

5. Conclusions

A facile self-assembly approach was successfully employed to produce mannose-decorated hybrid nanoparticles. Physicochemical characterization confirmed a stable and suitable nanocarrier system with efficient delivery properties. Spontaneous cell lysate and cellular uptake in U937 cells demonstrated that MDNPs with appropriate mannose density are highly favorable for the targeting of M2 macrophages more than M1 macrophages. Further, these nanoparticles did not exhibit cytotoxicity against U937 cells indicating that they possess biocompatibility characteristics. In conclusion, the MDNPs described in this study not only target macrophages, but also display safe profiles which can be utilized for the delivery of therapeutics for the treatment of inflammatory diseases, HIV-1, and for cancer therapy. However, further biological consequences of MDNPs still need to be evaluated for the delivery of therapeutics to be proven relevant in both in vitro and in vivo models.

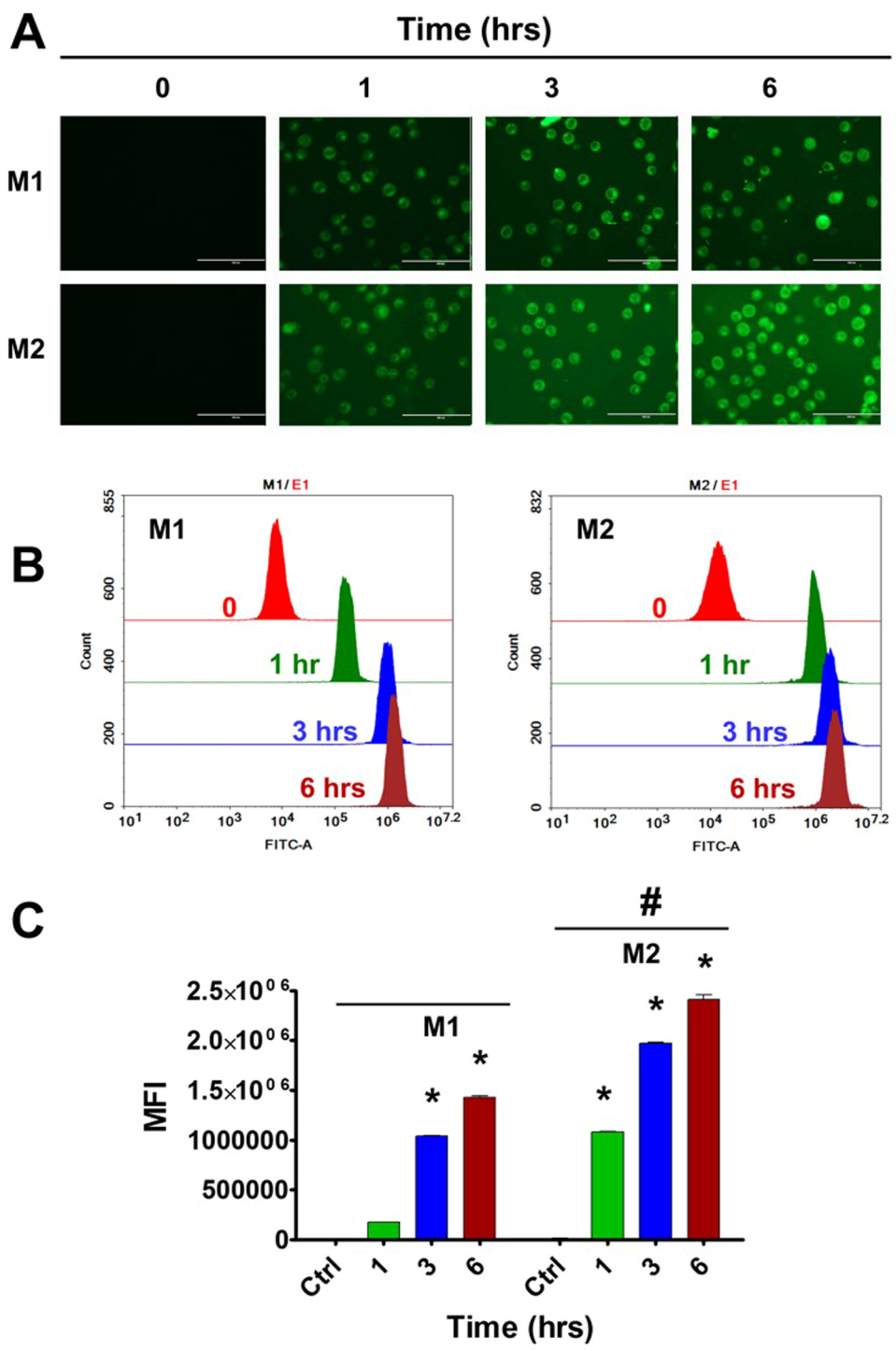

Fig. 4. MDNPs conveyed time-dependent cellular uptake in U937 cell line-differentiated M1 and M2 macrophages. 5×10^5 cells were treated with (A) 200 μg/mL mannose density on MDNPs (C6 concentration as 5 μg/mL) for 1–6 h. **(B-C)** Then cellular uptake information was acquired by EVOS® FL Imaging System and NovoCyte Flow Cytometer as mentioned in Fig. 3. The mean fluorescence intensity (MFI) values were presented as data are mean ± SEM (n = 3). Significant p-values (< 0.05) are represented as "*" different mannose density treated cells compared to control cells. Significant p-value (< 0.05) is represented as "#" M2 cells compared to M1 at individual mannose density treatment.

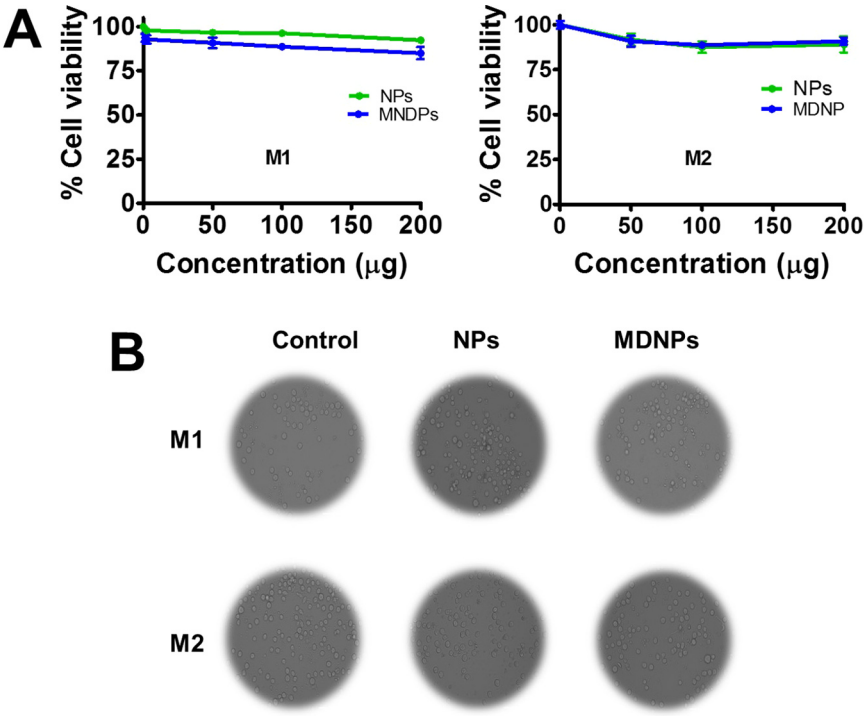

Fig. 5. MDNPs exhibits cytocompatibility on U937 cells. 5×10^3 cells were treated with 0–400 μg/mL 0-200 μg/mL F127-TA core NPs or MDNPs for **(A)** 24 h. After treatment, cells were incubated with 20 μL MTS reagent (CellTiter 96® AQueous, Promega, Madison, WI) for 2 h to measure cell viability compared to control cells (no treatment group). Data are mean ± SEM (n = 3). **(B)** Representative U937 cell images of above treatment groups were acquired using EVOS® FL Imaging System (AMF4300, Life Technologies, Carlsbad, CA, USA).

CRediT authorship contribution statement

Elham Hatami: Methodology, Validation, Formal analysis, Investigation, Data curation, Writing - original draft, Writing - review & editing, Visualization. **Ying Mu:** Methodology, Validation, Investigation, Data curation. **Deanna N. Shields:** Methodology, Validation, Data curation. **Subhash C. Chauhan:** Resources, Writing - review & editing, Funding acquisition. **Santosh Kumar:** Resources, Writing - review & editing, Funding acquisition. **Theodore J. Cory:** Conceptualization, Methodology, Formal analysis, Investigation, Resources, Writing - original draft, Writing - review & editing, Supervision, Project administration, Funding acquisition. **Murali M. Yallapu:** Conceptualization, Methodology, Formal analysis, Investigation, Resources, Writing - original draft, Writing - review & editing, Visualization, Supervision, Project administration, Funding acquisition.

Acknowledgments

Authors acknowledge support from UTHSC Molecular Resource Center (Fluorescence measurements), UTHSC Office of Research (Editorial Assistance), College of Pharmacy-UTHSC Shared Instrument and Flow cytometry Facility (FTIR and flow cytometry), and Department of Chemistry (University of Nebraska Medical Center, Lincoln, NE) (TGA analysis). MMY acknowledges Dr. Bilal Hafeez for scientific discussions.

Conflicts of interest

The authors declare no conflict of interest. The funders had no role in the design of the study; in the collection, analyses, or interpretation of data; in the writing of the manuscript, or in the decision to publish the results.

Funding

This research was supported by National Institute of Health/ National Cancer Center's Career Development Award (K22CA174841), AREA grant (CA213232), a UTHSC-CORNET, NEW GRANT, and College of Pharmacy Dean's Seed Grant to MMY. This work was also partially supported by the National Institutes of Health Research Project Grant Program (R01 CA210192, R01 CA206069, and CA204552 to SCC and R01 DA047178 to TJC and SK)

Appendix A. Transparency document

Supplementary data associated with this article can be found in the online version at doi:10.1016/j.bbrep.2019.01.007

References

[1] J.A. Van Ginderachter, K. Movahedi, J. Van den Bossche, P. De Baetselier, Macrophages, PPARs, and cancer, PPAR Res. 2008 (2008) 169414.
[2] B.S. Murphy, H.M. Bush, V. Sundareshan, C. Davis, J. Hagadone, T.J. Cory, H. Hoy, D. Hayes Jr., M.I. Anstead, D.J. Feola, Characterization of macrophage activation states in patients with cystic fibrosis, J. Cyst. Fibros. 9 (5) (2010) 314–322.
[3] C. Troidl, H. Mollmann, H. Nef, F. Masseli, S. Voss, S. Szardien, M. Willmer, A. Rolf, J. Rixe, K. Troidl, S. Kostin, C. Hamm, A. Elsasser, Classically and alternatively activated macrophages contribute to tissue remodelling after myocardial infarction, J. Cell. Mol. Med. 13 (9B) (2009) 3485–3496.
[4] A. Kumar, W. Abbas, G. Herbein, HIV-1 latency in monocytes/macrophages, Viruses 6 (4) (2014) 1837–1860.
[5] A. Mantovani, C. Garlanda, M. Locati, Macrophage diversity and polarization in atherosclerosis: a question of balance, Arterioscler. Thromb. Vasc. Biol. 29 (10) (2009) 1419–1423.
[6] A. Mantovani, M. Locati, Orchestration of macrophage polarization, Blood 114 (15) (2009) 3135–3136.
[7] A. Mantovani, A. Sica, S. Sozzani, P. Allavena, A. Vecchi, M. Locati, The chemokine system in diverse forms of macrophage activation and polarization, Trends Immunol. 25 (12) (2004) 677–686.
[8] B. Arnaiz, O. Martinez-Avila, J.M. Falcon-Perez, S. Penades, Cellular uptake of gold nanoparticles bearing HIV gp120 oligomannosides, Bioconjugate Chem. 23 (4) (2012) 814–825.
[9] F. Chiodo, P.M. Enriquez-Navas, J. Angulo, M. Marradi, S. Penades, Assembling different antennas of the gp120 high mannose-type glycans on gold nanoparticles provides superior binding to the anti-HIV antibody 2G12 than the individual antennas, Carbohydr. Res. 405 (2015) 102–109.
[10] F.S. Coulibaly, M.J.M. Ezoulin, S.S. Purohit, N.J. Ayon, N.A. Oyler, B.C. Youan, Layer-by-layer engineered microbicide drug delivery system targeting HIV-1gp120: physicochemical and biological properties, Mol. Pharm. 14 (10) (2017) 3512–3527.
[11] T. Dutta, H.B. Agashe, M. Garg, P. Balakrishnan, M. Kabra, N.K. Jain, Poly

(propyleneimine) dendrimer based nanocontainers for targeting of efavirenz to human monocytes/macrophages in vitro, J. Drug Target. 15 (1) (2007) 89–98.
[12] V. Gajbhiye, N. Ganesh, J. Barve, N.K. Jain, Synthesis, characterization and targeting potential of zidovudine loaded sialic acid conjugated-mannosylated poly (propyleneimine) dendrimers, Eur. J. Pharm. Sci.: Off. J. Eur. Fed. Pharm. Sci. 48 (4–5) (2013) 668–679.
[13] Y. Guo, C. Sakonsinsiri, I. Nehlmeier, M.A. Fascione, H. Zhang, W. Wang, S. Pohlmann, W.B. Turnbull, D. Zhou, Compact, polyvalent mannose quantum dots as sensitive, ratiometric FRET probes for multivalent protein-ligand interactions, Angew. Chem. 55 (15) (2016) 4738–4742.
[14] S.K. Jain, Y. Gupta, A. Jain, A.R. Saxena, P. Khare, A. Jain, Mannosylated gelatin nanoparticles bearing an anti-HIV drug didanosine for site-specific delivery, Nanomed.: Nanotechnol. Biol. Med. 4 (1) (2008) 41–48.
[15] T. Malik, G. Chauhan, G. Rath, R.N. Kesarkar, A.S. Chowdhary, A.K. Goyal, Efaverinz and nano-gold-loaded mannosylated niosomes: a host cell-targeted topical HIV-1 prophylaxis via thermogel system, Artif. Cells Nanomed. Biotechnol. (2017) 1–12.
[16] B.K. Patel, R.H. Parikh, N. Patel, Targeted delivery of mannosylated-PLGA nanoparticles of antiretroviral drug to brain, Int. J. Nanomed. 13 (2018) 97–100.
[17] E.B. Basalious, R.N. Shamma, Novel self-assembled nano-tubular mixed micelles of Pluronics P123, Pluronic F127 and phosphatidylcholine for oral delivery of nimodipine: In vitro characterization, ex vivo transport and in vivo pharmacokinetic studies, Int. J. Pharm. 493 (1–2) (2015) 347–356.
[18] S.M. Moghimi, A.C. Hunter, J.C. Murray, Long-circulating and target-specific nanoparticles: theory to practice, Pharmacol. Rev. 53 (2) (2001) 283–318.
[19] M.H. Wang, J.H. Jeong, J.C. Kim, Thermo-triggerable self-assembly comprising cinnamoyl polymeric beta cyclodextrin and cinnamoyl Pluronic F127, Colloids Surf. B Biointerfaces 142 (2016) 148–158.
[20] D.V. Mendonca, L.M. Lage, D.P. Lage, M.A. Chavez-Fumagalli, F. Ludolf, B.M. Roatt, D. Menezes-Souza, A.A. Faraco, R.O. Castilho, C.A. Tavares, J.M. Barichello, M.C. Duarte, E.A. Coelho, Poloxamer 407 (Pluronic((R)) F127)-based polymeric micelles for amphotericin B: In vitro biological activity, toxicity and in vivo therapeutic efficacy against murine tegumentary leishmaniasis, Exp. Parasitol. 169 (2016) 34–42.
[21] P.K. Singh, V.K. Pawar, A.K. Jaiswal, Y. Singh, C.H. Srikanth, M. Chaurasia, H.K. Bora, K. Raval, J.G. Meher, J.R. Gayen, A. Dube, M.K. Chourasia, Chitosan coated PluronicF127 micelles for effective delivery of Amphotericin B in experimental visceral leishmaniasis, Int. J. Biol. Macromol. 105 (Pt 1) (2017) 1220–1231.
[22] Y. Cai, J. Zhang, N.G. Chen, Z. Shi, J. Qiu, C. He, M. Chen, Recent advances in anticancer activities and drug delivery systems of tannins, Med. Res. Rev. 37 (4) (2017) 665–701.
[23] P. Chowdhury, P.K.B. Nagesh, S. Khan, B.B. Hafeez, S.C. Chauhan, M. Jaggi, M.M. Yallapu, Development of polyvinylpyrrolidone/paclitaxel self-assemblies for breast cancer, Acta Pharm. Sin. B 8 (4) (2018) 602–614.
[24] S.R. Abulateefeh, M.O. Taha, Enhanced drug encapsulation and extended release profiles of calcium-alginate nanoparticles by using tannic acid as a bridging cross-linking agent, J. Microencapsul. 32 (1) (2015) 96–105.
[25] B. Han, J. Jaurequi, B.W. Tang, M.E. Nimni, Proanthocyanidin: a natural cross-linking reagent for stabilizing collagen matrices, J. Biomed. Mater. Res. Part A 65 (1) (2003) 118–124.
[26] M. Besharati, A. Taghizadeh, Effect of tannin-binding agents (polyethylene glycol and polyvinylpyrrolidone) supplementation on in vitro gas production kinetics of some grape yield byproducts, ISRN Vet. Sci. 2011 (2011) 780540.
[27] S.H. Khoo, P.G. Hoggard, I. Williams, E.R. Meaden, P. Newton, E.G. Wilkins, A. Smith, J.F. Tjia, J. Lloyd, K. Jones, N. Beeching, P. Carey, B. Peters, D.J. Back, Intracellular accumulation of human immunodeficiency virus protease inhibitors, Antimicrob. Agents Chemother. 46 (10) (2002) 3228–3235.
[28] K. Jones, P.G. Hoggard, S. Khoo, B. Maher, D.J. Back, Effect of alpha1-acid glycoprotein on the intracellular accumulation of the HIV protease inhibitors saquinavir, ritonavir and indinavir in vitro, Br. J. Clin. Pharmacol. 51 (1) (2001) 99–102.
[29] H. He, M. Buckley, B. Britton, Y. Mu, K. Warner, S. Kumar, T.J. Cory, Polarized macrophage subsets differentially express the drug efflux transporters MRP1 and BCRP, resulting in altered HIV production, Antivir. Chem. Chemother. 26 (2018) (2040206617745168).
[30] T.J. Cory, H. He, L.C. Winchester, S. Kumar, C.V. Fletcher, Alterations in P-glycoprotein expression and function between macrophage subsets, Pharm. Res. (2016).
[31] P.K.B. Nagesh, P. Chowdhury, E. Hatami, V.K.N. Boya, V.K. Kashyap, S. Khan, B.B. Hafeez, S.C. Chauhan, M. Jaggi, M.M. Yallapu, miRNA-205 nanoformulation sensitizes prostate cancer cells to chemotherapy, Cancers 10 (9) (2018).
[32] P. Chowdhury, P.K.B. Nagesh, E. Hatami, S. Wagh, N. Dan, M.K. Tripathi, S. Khan, B.B. Hafeez, B. Meibohm, S.C. Chauhan, M. Jaggi, M.M. Yallapu, Tannic acid-inspired paclitaxel nanoparticles for enhanced anticancer effects in breast cancer cells, J. Colloid Interface Sci. 535 (2018) 133–148.
[33] T. Masuko, A. Minami, N. Iwasaki, T. Majima, S. Nishimura, Y.C. Lee, Carbohydrate analysis by a phenol-sulfuric acid method in microplate format, Anal. Biochem. 339 (1) (2005) 69–72.
[34] M.M. Yallapu, N. Chauhan, S.F. Othman, V. Khalilzad-Sharghi, M.C. Ebeling, S. Khan, M. Jaggi, S.C. Chauhan, Implications of protein corona on physico-chemical and biological properties of magnetic nanoparticles, Biomaterials 46 (2015) 1–12.
[35] X. Hu, Y. Shi, P. Zhang, M. Miao, T. Zhang, B. Jiang, d-mannose: properties, production, and applications, Overv. Comp. Rev. Food Sci. Food Saf. 15 (4) (2016).
[36] A.K. Azad, M.V. Rajaram, L.S. Schlesinger, Exploitation of the macrophage mannose receptor (CD206) in infectious disease diagnostics and therapeutics, J. Cytol. Mol. Biol. 1 (1) (2014).
[37] L. Martinez-Pomares, The mannose receptor, J. Leukoc. Biol. 92 (6) (2012) 1177–1186.
[38] U. Gazi, L. Martinez-Pomares, Influence of the mannose receptor in host immune responses, Immunobiology 214 (7) (2009) 554–561.
[39] A. Stimac, S. Segota, M. Dutour Sikiric, R. Ribic, L. Frkanec, V. Svetlicic, S. Tomic, B. Vranesic, R. Frkanec, Surface modified liposomes by mannosylated conjugates anchored via the adamantyl moiety in the lipid bilayer, Biochim. Biophys. Acta 1818 (9) (2012) 2252–2259.
[40] A.C. Vieira, L.L. Chaves, M. Pinheiro, D. Ferreira, B. Sarmento, S. Reis, Design and statistical modeling of mannose-decorated dapsone-containing nanoparticles as a strategy of targeting intestinal M-cells, Int. J. Nanomed. 11 (2016) 2601–2617.
[41] R.R. Arvizo, K. Giri, D. Moyano, O.R. Miranda, B. Madden, D.J. McCormick, R. Bhattacharya, V.M. Rotello, J.P. Kocher, P. Mukherjee, Identifying new therapeutic targets via modulation of protein corona formation by engineered nanoparticles, PLoS One 7 (3) (2012) e33650.
[42] K. Giri, K. Shameer, M.T. Zimmermann, S. Saha, P.K. Chakraborty, A. Sharma, R.R. Arvizo, B.J. Madden, D.J. McCormick, J.P. Kocher, R. Bhattacharya, P. Mukherjee, Understanding protein-nanoparticle interaction: a new gateway to disease therapeutics, Bioconjugate Chem. 25 (6) (2014) 1078–1090.
[43] E.M. Bruscia, P.X. Zhang, E. Ferreira, C. Caputo, J.W. Emerson, D. Tuck, D.S. Krause, M.E. Egan, Macrophages directly contribute to the exaggerated inflammatory response in cystic fibrosis transmembrane conductance regulator-/- mice, Am. J. Respir. Cell Mol. Biol. 40 (3) (2009) 295–304.
[44] O. Krysko, G. Holtappels, N. Zhang, M. Kubica, K. Deswarte, L. Derycke, S. Claeys, H. Hammad, G.G. Brusselle, P. Vandenabeele, D.V. Krysko, C. Bachert, Alternatively activated macrophages and impaired phagocytosis of S. aureus in chronic rhinosinusitis, Allergy 66 (3) (2011) 396–403.
[45] E. Cassol, L. Cassetta, M. Alfano, G. Poli, Macrophage polarization and HIV-1 infection, J. Leukoc. Biol. 87 (4) (2010) 599–608.
[46] E. Cassol, M. Alfano, P. Biswas, G. Poli, Monocyte-derived macrophages and myeloid cell lines as targets of HIV-1 replication and persistence, J. Leukoc. Biol. 80 (5) (2006) 1018–1030.
[47] M. Benoit, B. Desnues, J.L. Mege, Macrophage polarization in bacterial infections, J. Immunol. 181 (6) (2008) 3733–3739.
[48] S. Bhatia, M. Fei, M. Yarlagadda, Z. Qi, S. Akira, S. Saijo, Y. Iwakura, N. van Rooijen, G.A. Gibson, C.M. Croix St, A. Ray, P. Ray, Rapid host defense against Aspergillus fumigatus involves alveolar macrophages with a predominance of alternatively activated phenotype, PLoS One 6 (1) (2011) e15943.
[49] E. Klimcakova, B. Roussel, Z. Kovacova, M. Kovacikova, M. Siklova-Vitkova, M. Combes, J. Hejnova, P. Decaunes, J.J. Maoret, T. Vedral, N. Viguerie, V. Bourlier, A. Bouloumie, V. Stich, D. Langin, Macrophage gene expression is related to obesity and the metabolic syndrome in human subcutaneous fat as well as in visceral fat, Diabetologia 54 (4) (2011) 876–887.
[50] K. Movahedi, D. Laoui, C. Gysemans, M. Baeten, G. Stange, J. Van den Bossche, M. Mack, D. Pipeleers, P. In't Veld, P. De Baetselier, J.A. Van Ginderachter, Different tumor microenvironments contain functionally distinct subsets of macrophages derived from Ly6C(high) monocytes, Cancer Res. 70 (14) (2010) 5728–5739.
[51] A.C. Labonte, A.C. Tosello-Trampont, Y.S. Hahn, The role of macrophage polarization in infectious and inflammatory diseases, Mol. Cells 37 (4) (2014) 275–285.
[52] D.J. Feola, B.A. Garvy, T.J. Cory, S.E. Birket, H. Hoy, D. Hayes Jr., B.S. Murphy, Azithromycin alters macrophage phenotype and pulmonary compartmentalization during lung infection with Pseudomonas, Antimicrob. Agents Chemother. 54 (6) (2010) 2437–2447.
[53] M.S. Meltzer, D.R. Skillman, P.J. Gomatos, D.C. Kalter, H.E. Gendelman, Role of mononuclear phagocytes in the pathogenesis of human immunodeficiency virus infection, Annu. Rev. Immunol. 8 (1) (1990) 169–194.
[54] A. Zalar, M.I. Figueroa, B. Ruibal-Ares, P. Bare, P. Cahn, M.M. de Bracco, L. Belmonte, Macrophage HIV-1 infection in duodenal tissue of patients on long term HAART, Antivir. Res. 87 (2) (2010) 269–271.
[55] S. Aquaro, C.F. Perno, E. Balestra, J. Balzarini, A. Cenci, M. Francesconi, S. Panti, F. Serra, N. Villani, R. Calio, Inhibition of replication of HIV in primary monocyte/macrophages by different antiviral drugs and comparative efficacy in lymphocytes, J. Leukoc. Biol. 62 (1) (1997) 138–143.
[56] J.H. Campbell, A.C. Hearps, G.E. Martin, K.C. Williams, S.M. Crowe, The importance of monocytes and macrophages in HIV pathogenesis, treatment, and cure, Aids 28 (15) (2014) 2175–2187.
[57] T.J. Cory, T.W. Schacker, M. Stevenson, C.V. Fletcher, Overcoming pharmacologic sanctuaries, Curr. Opin. HIV AIDS 8 (3) (2013) 190–195.
[58] H. Koppensteiner, R. Brack-Werner, M. Schindler, Macrophages and their relevance in Human Immunodeficiency Virus Type I infection, Retrovirology 9 (2012) 82.
[59] V. Le Douce, G. Herbein, O. Rohr, C. Schwartz, Molecular mechanisms of HIV-1 persistence in the monocyte-macrophage lineage, Retrovirology 7 (2010) 32.
[60] W. Abbas, M. Tariq, M. Iqbal, A. Kumar, G. Herbein, Eradication of HIV-1 from the macrophage reservoir: an uncertain goal? Viruses 7 (4) (2015) 1578–1598.
[61] P. Benaroch, E. Billard, R. Gaudin, M. Schindler, M. Jouve, HIV-1 assembly in macrophages, Retrovirology 7 (2010) 29.
[62] G. Herbein, A. Varin, The macrophage in HIV-1 infection: from activation to deactivation? Retrovirology 7 (2010) 33.
[63] F. Porcheray, B. Samah, C. Leone, N. Dereuddre-Bosquet, G. Gras, Macrophage activation and human immunodeficiency virus infection: HIV replication directs macrophages towards a pro-inflammatory phenotype while previous activation

modulates macrophage susceptibility to infection and viral production, Virology 349 (1) (2006) 112–120.

[64] M. Arainga, B. Edagwa, R.L. Mosley, L.Y. Poluektova, S. Gorantla, H.E. Gendelman, A mature macrophage is a principal HIV-1 cellular reservoir in humanized mice after treatment with long acting antiretroviral therapy, Retrovirology 14 (1) (2017) 17.

[65] U. Roy, J. McMillan, Y. Alnouti, N. Gautum, N. Smith, S. Balkundi, P. Dash, S. Gorantla, A. Martinez-Skinner, J. Meza, G. Kanmogne, S. Swindells, S.M. Cohen, R.L. Mosley, L. Poluektova, H.E. Gendelman, Pharmacodynamic and antiretroviral activities of combination nanoformulated antiretrovirals in HIV-1-infected human peripheral blood lymphocyte-reconstituted mice, J. Infect. Dis. 206 (10) (2012) 1577–1588.